Membrane-Induced Folding of the cAMP-Regulated Phosphoprotein Endosulfine-α[†]

John M. Boettcher,[‡] Kevin L. Hartman,[‡] Daniel T. Ladror,[‡] Zhi Qi,[‡,§] Wendy S. Woods,[||] Julia M. George,[||] and Chad M. Rienstra*[,‡,§,⊥]

Department of Chemistry, Center for Biophysics and Computational Biology, Department of Molecular and Integrative Physiology, and Department of Biochemistry, University of Illinois, Urbana, Illinois 61801

Received August 1, 2008; Revised Manuscript Received September 16, 2008

ABSTRACT: Endosulfine-α (ENSA) is a 121-residue cAMP-regulated phosphoprotein, originally identified as an endogenous regulator of ATP-sensitive potassium channels. ENSA has been implicated in the regulation of insulin secretion, and expression of ENSA is decreased in brains of both Alzheimer's disease (AD) and Down's syndrome patients. We recently described membrane-dependent interactions between ENSA and the Parkinson's disease associated protein α-synuclein. Here we characterize the conformational change in ENSA that occurs upon binding to membranes. Secondary chemical shift analysis demonstrates formation of four helices in the lipid-bound state that are not present in the absence of lipid. The helical structure is maintained in several different lipid mimetics (sodium dodecyl sulfate, dodecyl phosphocholine, lyso 1-palmitoyl phosphatidylglycerol, and phospholipid vesicles). Introduction of a mutation (S109E) to mimic PKA phosphorylation of ENSA leads to a perturbation of the fourth helix and disrupts the interaction with α-synuclein. These data establish ENSA as an intrinsically unstructured protein that adopts a stable structure upon membrane binding, properties it shares with its binding partner α-synuclein.

Endosulfine-α (ENSA)[1]is a small cytosolic protein belonging to the cAMP-regulated phosphoprotein (ARPP) family (*1*). It was originally identified as an endogenous regulator of ATP-sensitive potassium channels (K-ATP channels), which function as metabolic sensors in a variety of cell types, where they couple secretory activity to the availability of ATP (*2*). K-ATP channels are the molecular targets of sulfonylurea drugs, a class of compounds used widely in the treatment of type II diabetes (*3*). Sulfonylureas bind to the sulfonylurea receptor (SUR) regulatory subunits of K-ATP channels in the pancreatic β cell membrane, leading to closure of the channel pore. The resulting inhibition of K^+ currents causes membrane depolarization and activation of voltage-gated Ca^{2+} channels, triggering insulin release. These same channels mediate glucose-stimulated insulin secretion, because they are alternately inhibited and activated via binding of metabolically produced ATP or MgADP to the SUR subunits. In brain tissue, K-ATP channel closure is associated with neurotransmitter release (*4*).

Based on the identification of the SUR subunits as specific receptors for sulfonylurea drugs, the existence of endogenous ligands for these receptors was proposed, akin to the discovery of endorphins as endogenous ligands for opioid receptors (*5*). ENSA was thus purified from ovine brain in a biochemical screen for proteins that could compete with sulfonylurea drugs for binding to the K-ATP channel (*6*). Recombinant ENSA protein was shown to inhibit K^+ currents in reconstituted pancreatic K-ATP channels, leading to the proposal that ENSA might regulate insulin secretion (*7*). Recent studies have failed to observe localization of ENSA to rat pancreatic β cells, raising some doubts regarding its proposed role in insulin secretion (*8*). However, other reports have demonstrated regulation of ENSA expression by glucose in mesangial cells of the kidney (*9*), which also express K-ATP channels that are sensitive to sulfonylureas. Treatment of insulin-deficient rats with low doses of glibenclamide (to mimic the effects of increased ENSA expression) protected against the development of glomerulosclerosis, a typical complication of diabetes (*10*).

While the function of ENSA has not been analyzed in the brain, its expression varies significantly in several pathological and functional contexts. ENSA protein is greatly decreased in frontal cortex and cerebellum of Alzheimer's disease patients (*11*) and in Down's syndrome patients with Alzheimer's disease pathology (*12*). ENSA mRNA is down-regulated in rat hippocampus with long-term memory consolidation, but up-regulated with swimming-related stress (*13*). Recent studies suggest that modulation of K-ATP channel activity by oxidative stress contributes to the

[†] This work was supported by grants from the Research Corporation (Cottrell Scholars Award to C.M.R.), the University of Illinois, and the Branfman Family Foundation (to J.M.G.).

* To whom correspondence should be addressed. Mailing address: Department of Chemistry, University of Illinois at Urbana−Champaign, 600 S Mathews Ave., Box 50-6, Urbana, IL 61801. Tel: 217 244-4655. Fax: 217 244-3186. E-Mail: rienstra@scs.uiuc.edu.

[‡] Department of Chemistry.

[§] Center for Biophysics and Computational Biology.

[||] Department of Molecular and Integrative Physiology.

[⊥] Department of Biochemistry.

[1] Abbreviations: ARPP, cAMP-regulated phosphoprotein; AD, Alzheimer's disease; AS, α-synuclein; CD, circular dichroism; CSI, consensus chemical shift index; DPC, dodecyl phosphocholine; ENSA, endosulfine-α; IUPs, intrinsically unstructured proteins; K-ATP channel, ATP-dependent potassium channel; LPPG, lyso 1-palmitoyl phosphatidylglycerol; NOE, nuclear Overhauser effect; MLVs, multilamellar vesicles; PD, Parkinson's disease; PKA, protein kinase A; POPA, 1-palmitoyl 2-oleoyl phosphatidic acid; POPC, 1-palmitoyl 2-oleoyl phosphatidylcholine; SDS, sodium dodecyl sulfate; SUR, sulfonylurea receptor; SUV, single unilamellar vesicles.

10.1021/bi801450t CCC: $40.75
Published on Web 10/31/2008

differential vulnerability of midbrain dopamine neurons to neurodegeneration in Parkinson's disease (*14*), but a potential role for ENSA in this process has not been considered.

We recently identified ENSA in a screen for conformation-dependent binding partners of α-synuclein (AS), an activity-dependent inhibitor of synaptic neurotransmission (*15, 16*) that is associated with both familial (*17*−*21*) and sporadic (*22, 23*) Parkinson's disease. The two proteins were found to interact only in the presence of SDS micelles or small unilamellar vesicles (*24*), conditions known to promote a dramatic conformational shift in AS from random coil to α helix (*25*). We speculate that ENSA and AS interact physiologically in a membrane-dependent fashion to regulate neuronal excitability and synaptic vesicle release. Here we use a combination of solution NMR, circular dichroism spectroscopy, and gel exclusion chromatography to characterize the structure of lipid-bound ENSA and to investigate the potential effects of PKA phosphorylation on the lipid-dependent interactions of ENSA and AS.

EXPERIMENTAL PROCEDURES

Recombinant Protein Expression. For isotopically labeled protein, cultures were grown in M9 minimal media supplemented with 2 g of [^{13}C]glucose, 1 g of [^{15}N]ammonium chloride, 10 mg of biotin, 10 mg of thiamine, and 10 mL of [^{13}C,^{15}N]-Bioexpress (Cambridge Isotopes Laboratories, Inc., Andover, MA). The wild-type and S109E ENSA constructs were prepared in pET21 vector (Novagen). Protein expression was induced with isopropyl-β-D-thiogalactopyranoside (IPTG) at 30 °C, followed by alkaline lysis, boiling, and precipitation with 60% ammonium sulfate. Precipitates were resolubilized and purified by hydrophobic interaction chromatography on a HiPrep 16/10 Butyl Fast Flow Sepharose column (GE Biosciences) and eluted with decreasing salt. ENSA-containing fractions were pooled and concentrated, then subjected to high-resolution gel filtration chromatography (HiPrep 16/160 Sephacryl S-200, GE Biosciences).

Full-length, untagged AS protein was produced for NMR experiments according to published procedures (*26*). Protein concentrations were determined spectrophotometrically by measuring absorbance at 280 nm assuming molar extinction coefficients of 4470 and 5200 M^{-1} cm^{-1} for ENSA and AS, respectively.

Circular Dichroism Spectroscopy. Circular dichroism spectra were acquired on a Jasco J720 Spectropolarimeter at room temperature. Spectra were acquired on ENSA free in solution and in the presence of lyso 1-palmitoyl phosphatidylglycerol (LPPG), dodecyl phosphocholine (DPC), sodium dodecyl sulfate (SDS), and small unilamelar vesicles (SUV). In all samples, ENSA was at a concentration of 15 μM. The concentration of LPPG, DPC, and SDS was 20 mM. The concentration of the small unilamellar vesicles was 4 mg/mL.

NMR Spectroscopy. Solution NMR spectra were acquired at the NMR Facility (School of Chemical Sciences, University of Illinois at Urbana−Champaign) on a Varian INOVA 600 MHz spectrometer equipped with a 5 mm triple resonance (^{1}H−^{13}C−^{15}N) triaxial gradient probe, using VNMRJ version 2.1B with the BioPack suite of pulse programs released in early 2006. Two-dimensional ^{1}H−^{15}N heteronuclear single quantum coherence (HSQC) spectra were measured for an average of 2 h per spectrum, digitizing 512 points in the indirect ^{15}N dimension ($t_{1,max}$ = 232 ms). The standard suite of heteronuclear triple resonance 3D spectra (HNCO, HNCA, HNCACB, CBCA(CO)NH) was utilized to establish correlations among backbone resonances for the S109E sample. Measurement times for the 3D spectra were 12−48 h. In all spectra, the direct ^{1}H dimension was acquired over a ∼15 ppm bandwidth with an acquisition time ($t_{3,max}$) of at least 100 ms, using standard ^{15}N and ^{13}C decoupling methods. The HNCO spectrum was digitized with 64 points in the ^{13}C dimension and 48 points in the ^{15}N dimension ($t_{1,max}$ = 21 ms; $t_{2,max}$ = 22 ms). The HNCA spectrum was digitized with 64 points in the ^{15}N dimension and 48 points in the ^{15}N dimension ($t_{1,max}$ = 14 ms; $t_{2,max}$ = 22 ms). The HNCACB spectrum was digitized with 96 points in the ^{13}C dimension and 60 points in the ^{15}N dimension ($t_{1,max}$ = 8 ms; $t_{2,max}$ = 25 ms). The CBCA(CO)NH spectrum was digitized with 64 points in the ^{13}C dimension and 48 points in the ^{15}N dimension ($t_{1,max}$ = 5 ms; $t_{2,max}$ = 22 ms). Spectral widths were adjusted to cover the bandwidths of interest, using default parameters in the BioPack software. Steady-state heteronuclear {^{1}H}-^{15}N nuclear Overhauser effect (NOE) experiments were acquired on ^{15}N-labeled ENSA. {^{1}H}-^{15}N NOE spectra were acquired for ENSA in the free (10 °C) and SDS micelle-bound (>140:1 SDS to ENSA ratio, 25 °C) states. This included one spectrum with proton saturation and one without saturation during a 5 s relaxation delay. The acquisition time for each spectrum was ∼12 h.

Spectra were processed with NMRPipe (*27*) and analyzed in Sparky (*28*). The free state consisted of 0.5 mM ^{15}N,^{13}C-labeled-ENSA in 50 mM phosphate buffer, pH 7.4, 10% D_2O. All subsequent lipid mimetic solutions were prepared using the same buffer (pH ≈ 7.4) to minimize chemical shifts due to changes in pH or ionic composition during titrations. The titrations were performed by the addition of the lipid mimetic solution directly to the NMR tube. The SDS micelle-bound state of ENSA was prepared by addition of 750 mM SDS in 4.6 mL aliquots, achieving a final concentration of at least 70 mM, that is, a 140:1 molar ratio of SDS to ENSA. The LPPG micelle-bound state of ENSA was prepared by the addition of 120 mM LPPG solution in 40 μL aliquots, achieving a final concentration of at least 60 mM, a 120:1 molar ratio of LPPG to ENSA. DPC micelle-bound state of ENSA was prepared by the addition of 150 mM DPC solution in 29.5 μL aliquots, achieving a final concentration of at least 60 mM, a 120:1 molar ratio of DPC to ENSA. The SUV-bound ENSA sample started with a 0.15 mM ENSA sample, and a 54 mM SUV solution was added in 58.3 μL aliquots. The final concentration reached was 22 mM SUV concentration (250:1 phospholipids/ENSA molar ratio). The S109E mutant was prepared in the SDS micelle-bound state in the same manner as the wild-type ENSA and following similar stoichiometry. For all NMR experiments, ENSA (wild-type and S109E) was filtered (0.2 μm) and first examined in the unfolded state by HSQC experiments; immediately thereafter, lipid mimetic was added to prepare the bound state, and additional HSQC experiments were acquired to confirm the titration end point. During subsequent experiments and for spectra of the WT and S109E ENSA−AS interaction, natural abundance AS was titrated immediately thereafter to the SDS micelle-bound ENSA, and the proce-

dure previously described was followed (*24*). Sample lifetime under these conditions typically ranged from 5 to 7 days. HSQC spectra were acquired in between blocks of lengthier 3D experiments to confirm sample integrity. In all the lipid-bound samples, the concentration of lipid mimetic significantly exceeded its critical micelle concentration.

Vesicle Preparation. 1-Palmitoyl 2-oleoyl phosphatidylcholine (POPC) and 1-palmitoyl 2-oleoyl phosphatidic acid (POPA) in chloroform were purchased from Avanti Polar Lipids (Alabaster, AL). A thin film of 3:1 POPC and POPA mixture was evenly applied to the inside of a round-bottom flask under gentle N_2 stream and then allowed to fully evaporate over at least half an hour. The dry lipids were resuspended in 3.5 mL of low-salt STB buffer (7.7 mM Tris, 50 mM NaCl, 10 mM EDTA, pH 7.4) per 60 mg of lipids, followed by a 2-h sonication in a Branson 2510 bath sonicator (Branson Ultrasonics, Danbury, CT) (*29*). The solution was separated by ultracentrifugation at 55 000 rpm (∼125 000 × *g*) in a TLA 100.3 rotor for 2 h at 25 °C according to a previous protocol (*25*). The top two-thirds of the solution at this stage contained a significant amount of multilamellar vesicles (MLVs), as confirmed by HPLC (*30*). Preparative-scale HPLC was impractical for preparation of quantities of SUVs required for NMR studies. Rather, centrifugation at 85 000 rpm (∼300 000 × *g*) for 2.5 h separated SUVs from MLVs. To improve the yield of SUVs, the bottom one-third fraction was collected from several centrifuge tubes and sonicated for 2 h (*30*).

RESULTS

ENSA Is an Unfolded Protein in Solution and Forms a More Helical Structure in Complex with Lipid Mimetics. Solution NMR was previously used to characterize the structure of ENSA in aqueous buffer and in the presence of sodium dodecyl sulfate (SDS) micelles (*31*). In the absence of SDS, the spectra demonstrated all the anticipated features of an unfolded protein, including minimal dispersion of ^{1}H chemical shifts (Figure 1A), rapid and strongly temperature-dependent exchange of most amide proton sites with water (Figure 1B), and small secondary chemical shifts (*32*). Consensus chemical shift index (CSI) (*33*) analysis concurred that ENSA is a predominantly unfolded protein in aqueous buffer, possessing secondary structure only in one short helix (residues 32−36). Heteronuclear ^{1}H−^{15}N NOE experiments revealed low-order parameters throughout, consistent with this disordered state (data not shown). Closer examination of the secondary chemical shifts (Figure 2A) illustrates a small residual helicity among two other short stretches of residues.

In the presence of SDS, ENSA undergoes a prominent conformational change to a more helical structure (*31*). CSI and TALOS analysis (*33, 34*) indicated the formation of four helices, consisting of residues 34−39, 49−64, 68−78, and 106−114 (*31*). Secondary Cα chemical shifts (Figure 2B) further confirm the significance of the change. Heteronuclear ^{1}H−^{15}N NOE experiments in this case revealed strong steady-state enhancements for the region from residue 34 to residue 116; the terminal domains yielded weak negative NOE intensities, consistent with a lack of secondary structure. Within the ordered domain, the highest NOE enhancements were observed for residues within the four helices (data not shown).

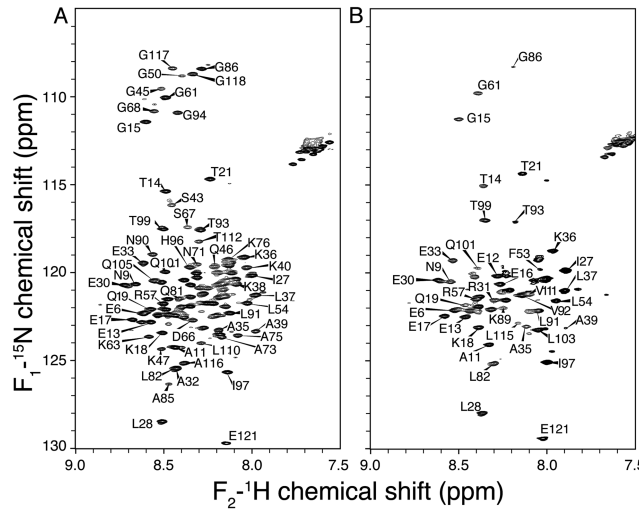

FIGURE 1: ^{15}N−^{1}H 2D HSQC NMR spectra of ENSA: (A) free (lacking detergent micelles) in solution at 10 °C (modified with permission from Figure 1 of ref *31*, copyright 2007 Springer); (B) free in solution at 25 °C. All the spectra were acquired with four scans per row and 512 rows and processed with sine bell apodization and zero filled in each dimension. Additional experimental details are reported in the text.

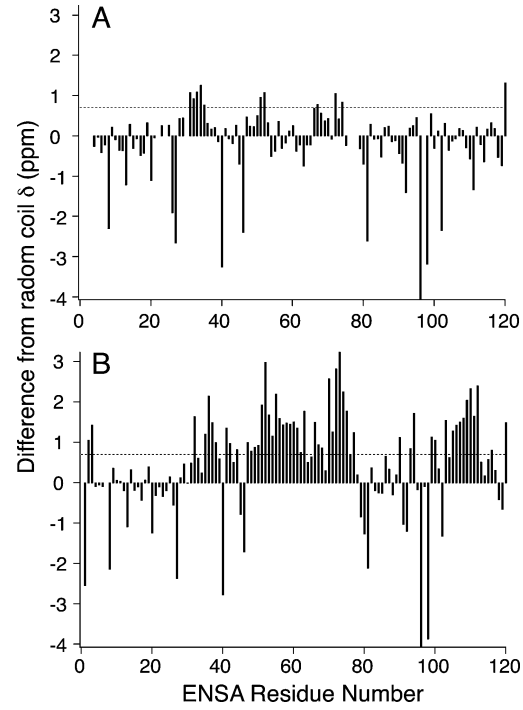

FIGURE 2: Secondary chemical shifts of α-carbons in ENSA: (A) ENSA in aqueous buffer; (B) ENSA bound to SDS micelles. Data are calculated as the deviation of the amino acid type-specific random coil value. Positive values indicate helical structure.

Gel Filtration Chromatography Confirms ENSA Binding to Phospholipid Membranes. The observation that ENSA undergoes a conformational change in the presence of SDS micelles suggested that ENSA might also interact with phospholipid bilayers, a more physiologically relevant membrane environment. We incubated ENSA (0.1 mg/mL) with small unilamellar phospholipid vesicles (SUV, 2 mg/mL) prepared at a ratio of 3:1 POPC/POPA and separated the mixture by gel filtration chromatography (Figure 3). Chromatograms of pure ENSA and pure SUV were acquired as controls. Pure ENSA eluted at ∼19 mL. The pure SUV

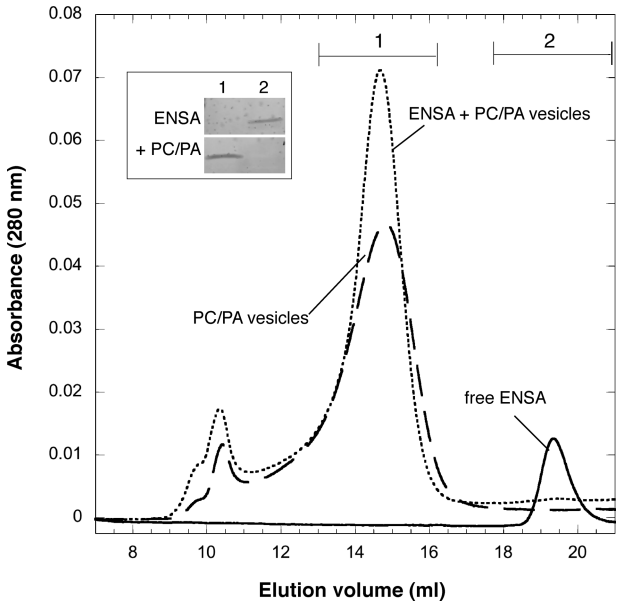

FIGURE 3: ENSA binds phospholipid vesicles. Vesicles (2 mg/mL) prepared from a 3:1 mixture of POPC and POPA were incubated 10 min with recombinant ENSA protein (0.1 mg/mL), and the mixture was separated by gel filtration chromatography (•••). For comparison, lipid-free ENSA protein (—) and pure vesicles (– – –) were subjected to similar separation. Pooled fractions (indicated by brackets) from the free ENSA and ENSA/lipid samples were separated by SDS−PAGE, stained with Coomassie blue, and visualized by scanning with the Odyssey infrared imaging system (inset).

solution eluted predominantly at 14.5 mL, with two smaller peaks (representing larger multilamellar vesicles) detected near 10 mL (*25*). Upon incubation with SUV, the free ENSA peak essentially disappeared, and the SUV peak increased in intensity, indicating binding of the protein to the phospholipid vesicles. Integration of peak areas in the presence and absence of vesicles indicated that >80% of the protein bound under these conditions. The SUV peak also eluted at a slightly lower elution volume, indicating an increase in the hydrodynamic radius of the vesicles upon protein binding. The MLV peaks were also shifted slightly, suggesting that ENSA binds these larger vesicles as well. The inset to Figure 3 shows SDS−polyacrylamide gel electrophoresis (PAGE) of pooled fractions representing the free protein peak (lane 2) and the SUV/ENSA peak (lane 1) to confirm the shift in ENSA elution time in the presence of SUV. These data confirm that ENSA binds phospholipid vesicles.

Far-UV Circular Dichroism Demonstrates Conformational Changes in the Presence of Lipid Mimetic. We next investigated the ENSA structure in complex with different membrane mimetics using far-UV circular dichroism (CD) spectroscopy, comparing the results to the SDS-induced structure. CD spectra were obtained for ENSA in the presence of micelles (SDS, dodecyl phosphocholine (DPC), or lyso 1-palmitoyl phosphatidylglycerol (LPPG)) and small unilamellar vesicles (SUV, 3:1 POPC/POPA). The CD spectra (Figure 4) agreed with the NMR analysis of SDS-bound ENSA, indicating little secondary structure for ENSA in the absence of lipid but significant increases in helical content in the presence of lipid mimetic; these structural elements are indicated by local minima at 208 and 222 nm (Figure 4). The CD spectra of ENSA in the presence of SDS and LPPG were very similar, indicating almost identical helical content for both, according to the intensity at 222 nm (*35*). The spectra obtained in the presence of DPC and SUV (Figure 4A,B) showed an increase in helical content over free ENSA but less than in the presence of SDS or LPPG.

HSQC Spectra Demonstrate Structural Changes of ENSA in the Presence of Several Lipid Mimetics. The specific conformational events driving the association with membranes were examined further by solution NMR spectroscopy of ^{15}N-ENSA in complex with the lipid mimetics (SDS, LPPG, DPC, and SUV) used previously for the CD experiments (Figure 5). In all cases, significant changes in the HSQC spectra are observed as the lipid mimetic-to-protein ratio is increased. In the limit of excess lipid or detergent (molar ratio greater than 100:1 SDS/ENSA, LPPG/ENSA, and DPC/ENSA and greater than 200:1 SUV/ENSA), no further changes of statistical significance occur, indicating that ENSA exists in the lipid-bound state if provided a sufficient excess of lipid mimetic. The HSQC spectra obtained in the presence of SDS, LPPG, and DPC at 25 °C (Figure 5A−C) demonstrate greater chemical shift dispersion than free ENSA (~1.4 ppm for SDS and LPPG, ~1.1 ppm for DPC), consistent with an increase in secondary structure throughout the protein. Temperature-dependent chemical shift changes were also greatly reduced in the micelle-bound states, indicative of decreases in the accessibility of the protein to bulk water, as expected when the protein folds.

Initial assignments were made of the spectra by observing changes from the free state assignments and during the course of the titrations with lipid mimetics. In the presence of SUV, many of the ENSA resonances broaden and become depressed in intensity, leaving only ~35 of the expected 112 resonances (Figure 5D) in the HSQC spectrum in the presence of SUVs. This is approximately half the number seen for ENSA in solution at 25 °C. The resonances remaining were assigned to the N and C termini, which are unstructured in the SDS micelle-bound samples (*31*). Likewise, in the presence of DPC and LPPG, the same ~45 peaks appear in similar regions of the spectrum and have chemical shifts consistent with random coil conformations. In addition to those signals that could be assigned straightforwardly, other resonances appeared at higher ratios of lipid to protein and therefore required *de novo* backbone assignment, which we performed for the SDS- and LPPG-bound states. The DPC spectra contained ~75 total peaks (excluding resonances associated with side chain amines), while both SDS and LPPG spectra contained ~110 resonances.

Assignment and Structural Interpretation of the LPPG Micelle-Bound ENSA NMR Data. We have previously reported the assignments of the SDS micelle-bound sample (*31*). To validate the significance of this conformation to the physiology of ENSA, we have further investigated this behavior with lysophospholipids and vesicles. The LPPG micelle is a better approximation of physiological lipids than is SDS, so it was of interest to assess whether ENSA assumes the same detailed structural properties in this context. Although the signals for the LPPG/ENSA complex were generally weaker and broader than the SDS micelle-bound ENSA (due to the larger size (~30 kDa) of the LPPG micelle) assignments were 80% complete. Resonances assigned to residues 6−30, 82−97, and 116−121 displayed high sensitivity and narrow line widths, which along with a

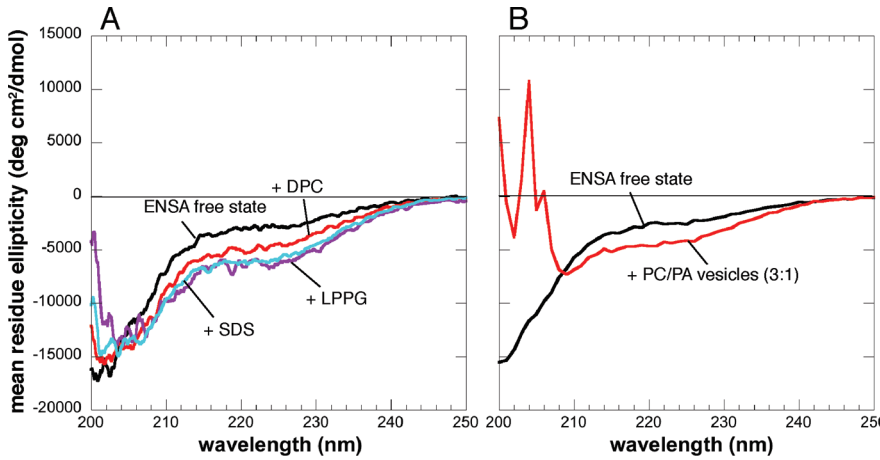

FIGURE 4: Far UV circular dichroism spectra plotted with mean residue ellipticity [Θ] as a function of wavelength for (A) ENSA free in solution (black), with excess SDS (light blue), with excess DPC (red), and with excess LPPG (purple) and (B) CD spectra of ENSA free in solution (black) and with excess SUV (red).

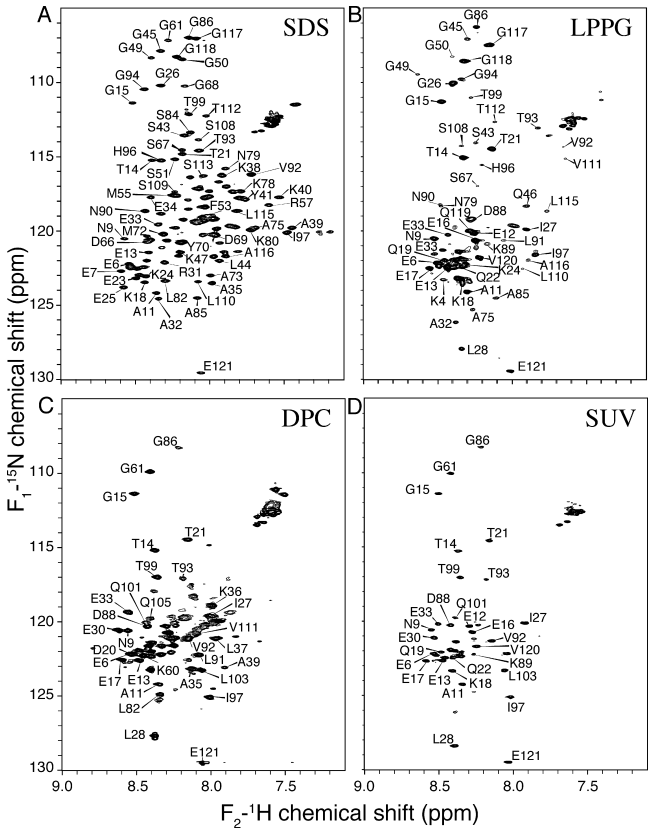

FIGURE 5: $^{15}N-^{1}H$ HSQC NMR spectrum of (A) SDS micelle-bound ENSA (modified with permission from Figure 1 of ref *31*, copyright 2007 Springer), (B) LPPG micelle-bound ENSA, (C) DPC micelle-bound ENSA, and (D) ENSA bound to SUV. HSQC spectra were acquired as a function of lipid mimetic concentration to confirm the end point of the titration. An excess of lipid mimetic was employed for all subsequent experiments. Experimental and processing parameters are identical to those in Figure 1.

lack of significant secondary shifts indicated that these regions of the protein are not directly bound to the micelle. Several other stretches of amino acids were assigned, despite depressed signal intensities, to regions within the same portions of the sequence that formed helices in the presence of SDS, and CSI analysis (*33*) for the assigned regions showed good agreement with the secondary structure domains observed in SDS. The helices found in the SDS micelle-bound sample are present in the LPPG micelle-bound

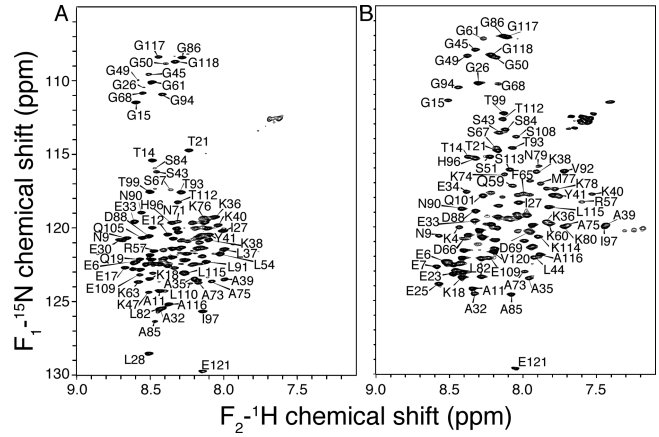

FIGURE 6: $^{15}N-^{1}H$ 2D HSQC NMR spectra of S109E-ENSA: (A) free (lacking detergent micelles) in solution at 10 °C; (B) SDS micelle-bound S109E-ENSA at 25 °C. Experimental and processing parameters are identical to those in Figure 1.

sample, including the formation of a helix that contains S109, the site of phosphorylation by protein kinase A (PKA) (*7*).

Figure 5 also illustrates that signals assigned in ENSA bound to SUV are consistent with random coil conformation. Resonances from residues bound to the SUV (and in helical conformation, based upon the CD results) are broadened beyond detection; therefore assignments were possible only for regions where ENSA is not tightly bound to the vesicle. These regions of the protein agree well with the disordered ENSA residues in the SDS, DPC, and LPPG complexes.

S109 Phosphorylation Affects the Interaction of ENSA with Membranes. The results of the previous experiments indicate that ENSA undergoes a conformational change upon binding to membranes that includes the formation of the four helices reported previously for SDS (*31*). An interesting feature of the membrane-bound structure of ENSA is the formation of a helix that contains the site of phosphorylation (S109) by PKA (*7*). To examine the effect of phosphorylation on the structure of membrane-bound ENSA, we investigated a phosphorylation mutant, S109E, by NMR. Initially, HSQC spectra for S109E were obtained in the absence of membrane mimetic at 10 °C (pH 7.5, Figure 6A). The spectra were highly similar to those for wild-type ENSA in solution and showed the same unstructured characteristics previously reported for wild-type ENSA (*31*). Assignments for the

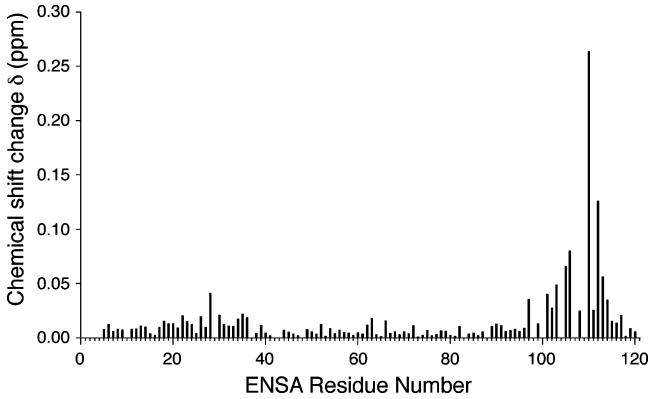

FIGURE 7: Chemical shift differences between detergent-bound forms of wild-type ENSA and the S109E mutant. N and HN differences were calculated for the 107 assigned residues in the HSQC spectra using the formula $\delta = ([0.1\delta_N]^2 + \delta_H^2)^{1/2}$, where δ_N and δ_H are the respective changes in ^{15}N and ^1H chemical shifts in the units of ppm.

S109E resonances in aqueous buffer therefore were presumed to be similar to the wild-type ENSA assignments and confirmed through a subset of 3D experiments. Regions showing significant chemical shift perturbations in the S109E mutant included not only the region near the mutation site but also residues 30−40; this region contains the only element of secondary structure observed for ENSA in solution (*31*), a helix from residue 32−36.

Next, NMR spectra were acquired on the S109E phosphorylation mutant of ENSA in the presence of saturating quantities of SDS (as confirmed by titrations as described above). HSQC (Figure 6B), HNCACB, HN(CO)CACB, and HNCO spectra were acquired for the S109E micelle-bound sample and unambiguous assignments of CA, CB, CO, N, and HN were obtained, from which the secondary structure could be inferred (*33*). The secondary structures are highly similar throughout the majority of the protein; however, the helix near the S109E mutation site is disrupted, containing only one helix turn (from residue 105 to residue 109) rather than three turns as observed in the wild-type protein. Chemical shift perturbation analysis (Figure 7) confirms that the only significant change in local conformation must occur near the C-terminus, although some of these conformational events may be allosterically transmitted to the short N-terminal helix. Most of these latter changes are on the order of 0.01−0.03 ppm, at the limit of significance for this experiment.

Previously, we used chemical shift perturbation mapping to explore the conformation dependence and structural specificity of the interaction of the neuronal protein α-synuclein (AS) and ENSA in the presence of SDS (*24*). Here we employ the same approach but with ^{15}N-labeled ENSA and natural abundance AS. The ENSA−AS interaction depends upon the helical conformation of each protein; therefore, we examined the effect of titrating SDS-bound AS into a preformed solution of SDS-bound ENSA. The chemical shift perturbations in ENSA were continuous and approximately linear in AS concentration (Figure 8A). At a 1:1 molar ratio ENSA/AS, several ENSA residues show substantial changes in chemical shift (>0.03 ppm), including K4, Q5, several residues among L28 to E34, K89, G94, H96, and I97. Other residues showed smaller changes (0.01−0.03 ppm), while a majority of residues indicated no conformational change with differences in chemical shift within the expected error of the experiments (<0.01 ppm). We also performed chemical shift perturbation mapping with the ENSA S109E mutant (Figure 8B). In contrast to the wild-type behavior, only four peaks are perturbed (L28, K63, Y64, and L103), at the borderline of statistical significance, indicative of a much weaker interaction between AS and the S109E ENSA mutant, as compared with wild-type ENSA.

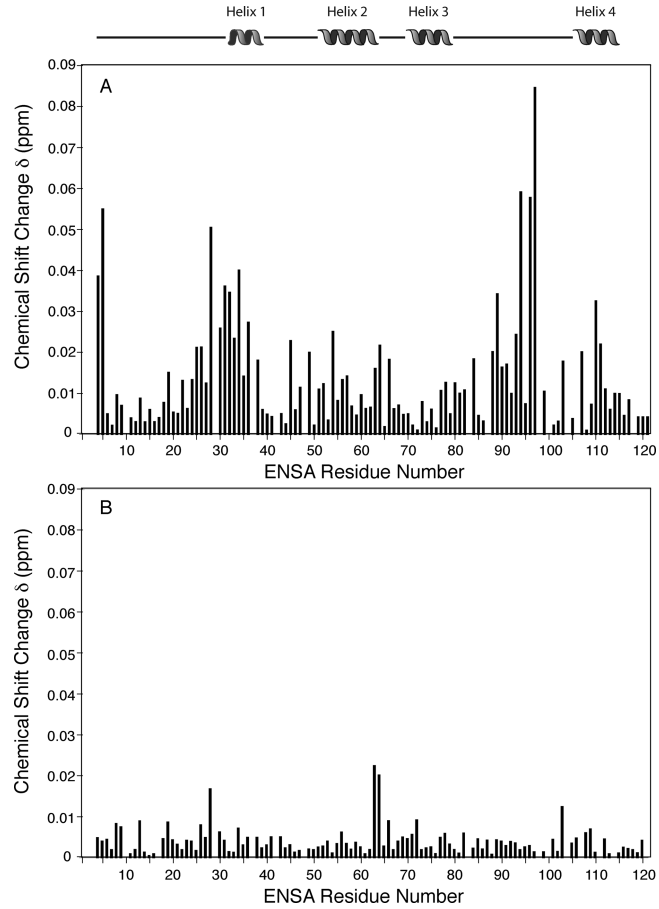

FIGURE 8: Chemical shift changes upon interaction of (A) micelle-bound wild-type ENSA with AS and (B) micelle-bound S109E-ENSA with AS. Chemical shift differences are reported as a function of residue number, where $\delta = ([0.1\delta_N]^2 + \delta_H^2)^{1/2}$ and δ_N and δ_H are the respective changes in ^{15}N and ^1H chemical shifts in the units of ppm. Superimposed is a cartoon representation of the CSI predicted secondary structure for wild-type membrane bound ENSA, with lines indicating random coil regions.

DISCUSSION

ENSA Forms a Helical Structure When Bound to Lipids. ENSA is a predominantly unfolded protein in aqueous solution with some nascent structure present. We find that ENSA undergoes a major structural rearrangement when bound to lipids such that the protein has well-defined secondary structure. We previously observed that residues ∼30 to ∼115 of ENSA, in the presence of SDS, adopt a helical structure (*31*). In the current study, we demonstrate further that the binding is not SDS-specific but that several lipid mimetics (DPC, LPPG, and POPC/POPA SUVs) cause a similar conformational change. In all cases, increased helicity is observed in CD spectra (based upon ellipticity at 222 nm), which is confirmed by $^1H-^{15}N$ HSQC NMR spectra for the micelles. Furthermore, the $^1H-^{15}N$ HSQC

spectra of ENSA in the presence of SUVs show strong signals for only the disordered termini and loops; residues bound tightly to the vesicle tumble too slowly for conventional solution NMR spectra to yield narrow resonance lines (residues 30−116). Thus the observed resonances in the spectra of SUV-bound samples were assigned to the N and C termini, correlating well with the regions that are unstructured in both the SDS- and LPPG-bound samples. The remainder of the protein is, as expected from the other mimetics, helical. Thus all evidence consistently reports a secondary structure change throughout approximately one-third of the protein. Like ENSA, the homologous protein ARPP-19 (∼87% sequence homology) was also reported to be largely unstructured in solution (*36*). Given the strong sequence similarity between ENSA and ARPP-19, it is likely that ARPP-19 undergoes a similar conformational change upon lipid binding.

The Helical Regions of Lipid-Bound ENSA Are Rich in Basic Residues. Like other peripheral membrane proteins (*37*), ENSA contains large numbers of positively charged residues and preferentially binds lipids that contain anionic head groups. The four helices that form in the membrane-bound state correspond to regions of the protein rich in positively charged amino acids. For example, helix 1 contains residues K36 and K38; in addition, R31 and K40 are at either end of the helix. The second and third helices are rich in basic residues (K56, R57, K60, K63, K74, K76, and K78). Likewise, the fourth helix contains R106, K107, and K114.

The involvement of positively charged amino acids likely accounts for the higher affinity of ENSA for lipids with anionic head groups, as illustrated by comparison of the spectra in complex with anionic SDS and zwitterionic DPC micelle-bound ENSA. Both detergents have the same length side chain and form micelles of ∼20 kDa. While CD data indicated that binding to both mimetics increased the helical content of ENSA, the SDS-bound state showed a more robust change to helical conformation (Figure 4A), in agreement with data obtained for LPPG, also bearing an anionic headgroup. In the NMR data, additional resonances were observed for the SDS micelle-bound sample (∼110) compared with the DPC-bound sample (∼75), and the resonances in the DPC-bound state were broader, which we attribute to intermediate exchange of the helices on and off the micelle.

PKA Phosphorylation May Regulate the ENSA−AS Interaction. As previously shown (*24*), AS must be in a helical conformation in order to interact with ENSA, and here we have shown that ENSA also adopts a helical conformation as a prerequisite to AS binding. Here we extended this idea by evaluating the role of phosphorylation in ENSA−AS interactions. Phosphorylation is a common mechanism for regulation of protein−protein interactions, and it is known that PKA phosphorylates S109 of ENSA (*7*). Thus we investigated the S109E mutant, a mimic of phosphorylated ENSA, and found that the fourth helix was disrupted and interactions with AS were significantly attenuated. Chemical shift perturbation measurements indicated that the binding of AS to wild-type ENSA primarily involves ENSA residues 28−36 and 88−97 (Figure 8), with smaller but still significant perturbations involving residues near S109. In contrast, no chemical shift perturbations of significance are observed in the S109E mutant of ENSA upon titration with AS.

Significance of Lipid Binding to ENSA Function. K-ATP channels are found at the plasma membrane and at intracellular membranes including the endoplasmic reticulum, secretory granules, and mitochondrial membranes (*38*). The SUR1 and SUR2 regulatory subunits of K-ATP channels are oriented toward the cytoplasmic membrane face, and sulfonylurea drugs are thought to exert their effects intracellularly after first crossing the plasma membrane (*39*). Likewise, ENSA is localized to the cytoplasm, where it is proposed to bind the SUR subunits and thereby modulate the K-ATP channel conductance (*8, 9*). Here we show that ENSA is also a lipid-binding protein and that lipid interactions alter folding. We propose that the local membrane environment may regulate the interaction between ENSA and the SUR subunits of the K-ATP channel.

CONCLUSION

Here we have demonstrated that ENSA belongs to the class of intrinsically unstructured proteins (IUPs), which show little to no tertiary structure in isolation but assume function in concert with a conformational change induced by interaction with target molecules. IUPs thereby exhibit biological properties that are not found in their highly structured counterparts. For example, IUPs can bind to multiple target molecules due to the plasticity of their structure (*40*). Induction of tertiary structure upon target binding can enhance specificity while keeping the binding affinity low (*40*), enabling interactions with multiple partners and sometimes producing disparate physiological effects. Because of these properties, IUPs often display complex regulatory properties in signaling networks (*41*).

In the case of ENSA, published studies suggest a role in the regulation of K-ATP channels, which are central to the physiological regulation of insulin secretion (*2*). Other studies, including our own, implicate ENSA in brain physiology (*13, 24*), where its loss is associated with neurodegeneration (*11, 12*). We propose that ENSA may participate in multiple physiological processes, involving multiple binding partners, by virtue of its intrinsic structural plasticity. ENSA may partner functionally with AS (also a lipid-stabilized IUP (*25*)) in neural tissue to subserve a neural-specific function and yet also partner with other molecules in different cellular contexts. As with many other regulatory proteins, these interactions are modified by phosphorylation. The structural data reported here begin to clarify the importance of environmental effects on ENSA structure and will facilitate a better understanding of the role ENSA plays in diverse processes from insulin secretion to neurodegeneration.

ACKNOWLEDGMENT

We thank Kathryn Kloepper and Dr. Donghua Zhou for their help in the initial stages of this project, and we also acknowledge Dr. Zhou's assistance with vesicle preparation.

REFERENCES

1. Peyrollier, K., Heron, L., Virsolvy-Vergine, A., LeCam, A., and Bataille, D. (1996) Alpha endosulfine is a novel molecule, structurally related to a family of phosphoproteins. *Biochem. Biophys. Res. Commun. 223*, 583–586.
2. Nichols, C. G. (2006) K-ATP channels as molecular sensors of cellular metabolism. *Nature 440*, 470–476.

3. Ashcroft, S. J. H. (2000) The beta-cell K-ATP channel. *J. Membr. Biol. 176*, 187–206.
4. Lee, K., Brownhill, V., and Richardson, P. J. (1997) Antidiabetic sulphonylureas stimulate acetylcholine release from striatal cholinergic interneurones through inhibition of K-ATP channel activity. *J. Neurochem. 69*, 1774–1776.
5. Lupo, B., and Bataille, D. (1987) A binding-Site for [3H] glipizide in the rat cerebral-cortex. *Eur. J. Pharmacol. 140*, 157–169.
6. Virsolvy-Vergine, A., Leray, H., Kuroki, S., Lupo, B., Dufour, M., and Bataille, D. (1992) Endosulfine, an endogenous peptidic ligand for the sulfonylurea receptor: purification and partial characterization from ovine brain. *Proc. Natl. Acad. Sci. U.S.A. 89*, 6629–6633.
7. Heron, L., Virsolvy, A., Peyrollier, K., Gribble, F. M., Le Cam, A., Ashcroft, F. M., and Bataille, D. (1998) Human alpha endosulfine, a possible regulator of sulphonylurea-sensitive K-ATP channel. *Proc. Natl. Acad. Sci. U.S.A. 95*, 8387–8391.
8. Gros, L., Breant, B., Duchene, B., Leroy, C., Fauconnier, G., Bataille, D., and Virsolvy, A. (2002) Localization of alpha-endosulfine in pancreatic somatostatin delta cells and expression during rat pancreas development. *Diabetologia 45*, 703–710.
9. Yee, J., Cortes, P., Barnes, J. L., Alviani, R., Biederman, J. I., and Szamosfalvi, B. (2004) Rat mesangial alpha-endosulfine. *Kidney Int. 65*, 1731–1739.
10. Biederman, J. I., Vera, E., Pankhaniya, R., Hasset, C., Giannico, G., Yee, J., and Cortes, P. (2005) Effects of sulfonylureas, alpha-endosulfine counterparts, on glomerulosclerosis in type 1 and type 2 models of diabetes. *Kidney Int. 67*, 554–565.
11. Kim, S. H., and Lubec, G. (2001) Brain alpha-endosulfine is manifold decreased in brains from patients with Alzheimer's disease: a tentative marker and drug target? *Neurosci. Lett. 310*, 77–80.
12. Kim, S. H., and Lubec, G. (2001) Decreased alpha-endosulfine, an endogenous regulator of ATP-sensitive potassium channels, in brains from adult Down syndrome patients. *J. Neural Transm. Suppl.* 1–9.
13. Dou, J. T., Cui, C. H., Dufour, F., Alkon, D. L., and Zhao, W. Q. (2003) Gene expression of alpha-endosulfine in the rat brain: correlative changes with aging, learning and stress. *J. Neurochem. 87*, 1086–1100.
14. Liss, B., Haeckel, O., Wildmann, J., Miki, T., Seino, S., and Roeper, J. (2005) K-ATP channels promote the differential degeneration of dopaminergic midbrain neurons. *Nat. Neurosci. 8*, 1742–1751.
15. Cabin, D. E., Shimazu, K., Murphy, D., Cole, N. B., Gottschalk, W., McIlwain, K. L., Orrison, B., Chen, A., Ellis, C. E., Paylor, R., Lu, B., and Nussbaum, R. L. (2002) Synaptic vesicle depletion correlates with attenuated synaptic responses to prolonged repetitive stimulation in mice lacking alpha-synuclein. *J. Neurosci. 22*, 8797–8807.
16. Abeliovich, A., Schmitz, Y., Farinas, I., Choi-Lundberg, D., Ho, W. H., Castillo, P. E., Shinsky, N., Verdugo, J. M. G., Armanini, M., Ryan, A., Hynes, M., Phillips, H., Sulzer, D., and Rosenthal, A. (2000) Mice lacking alpha-synuclein display functional deficits in the nigrostriatal dopamine system. *Neuron 25*, 239–252.
17. Chartier-Harlin, M. C., Kachergus, J., Roumier, C., Mouroux, V., Douay, X., Lincoln, S., Levecque, C., Larvor, L., Andrieux, J., Hulihan, M., Waucquier, N., Defebvre, L., Amouyel, P., Farrer, M., and Destee, A. (2004) Alpha-synuclein locus duplication as a cause of familial Parkinson's disease. *Lancet 364*, 1167–1169.
18. Kruger, R., Kuhn, W., Muller, T., Woitalla, D., Graeber, M., Kosel, S., Przuntek, H., Epplen, J. T., Schols, L., and Riess, O. (1998) Ala30Pro mutation in the gene encoding alpha-synuclein in Parkinson's disease. *Nat. Genet. 18*, 106–108.
19. Polymeropoulos, M. H., Lavedan, C., Leroy, E., Ide, S. E., Dehejia, A., Dutra, A., Pike, B., Root, H., Rubenstein, J., Boyer, R., Stenroos, E. S., Chandrasekharappa, S., Athanassiadou, A., Papapetropoulos, T., Johnson, W. G., Lazzarini, A. M., Duvoisin, R. C., DiIorio, G., Golbe, L. I., and Nussbaum, R. L. (2045) (1997) Mutation in the alpha-synuclein gene identified in families with Parkinson's disease. *Science 276*, 2045–2047.
20. Singleton, A. B., Farrer, M., Johnson, J., Singleton, A., Hague, S., Kachergus, J., Hulihan, M., Peuralinna, T., Dutra, A., Nussbaum, R., Lincoln, S., Crawley, A., Hanson, M., Maraganore, D., Adler, C., Cookson, M. R., Muenter, M., Baptista, M., Miller, D., Blancato, J., Hardy, J., and Gwinn-Hardy, K. (2003) Alpha-synuclein locus triplication causes Parkinson's disease. *Science 302*, 841–841.
21. Zarranz, J. J., Alegre, J., Gomez-Esteban, J. C., Lezcano, E., Ros, R., Ampuero, I., Vidal, L., Hoenicka, J., Rodriguez, O., Atares, B., Llorens, V., Tortosa, E. G., del Ser, T., Munoz, D. G., and de Yebenes, J. G. (2004) The new mutation, E46K, of alpha-synuclein causes Parkinson and Lewy body dementia. *Ann. Neurol. 55*, 164–173.
22. Spillantini, M. G., Schmidt, M. L., Lee, V. M. Y., Trojanowski, J. Q., Jakes, R., and Goedert, M. (1997) Alpha-synuclein in Lewy bodies. *Nature 388*, 839–840.
23. Irizarry, M. C., Growdon, W., Gomez-Isla, T., Newell, K., George, J. M., Clayton, D. F., and Hyman, B. T. (1998) Nigral and cortical Lewy bodies and dystrophic nigral neurites in Parkinson's disease and cortical Lewy body disease contain alpha-synuclein immunoreactivity. *J. Neuropathol. Exp. Neurol. 57*, 334–337.
24. Woods, W. S., Boettcher, J. M., Zhou, D. H., Kloepper, K. D., Hartman, K. L., Ladror, D. T., Qi, Z., Rienstra, C. M., and George, J. M. (2007) Conformation-specific binding of alpha-synuclein to novel protein partners detected by phage display and NMR spectroscopy. *J. Biol. Chem. 282*, 34555–34567.
25. Davidson, W. S., Jonas, A., Clayton, D. F., and George, J. M. (1998) Stabilization of alpha-synuclein secondary structure upon binding to synthetic membranes. *J. Biol. Chem. 273*, 9443–9449.
26. Kloepper, K. D., Woods, W. S., Winter, K. A., George, J. M., and Rienstra, C. M. (2006) Preparation of alpha-synuclein fibrils for solid-state NMR: Expression, purification, and incubation of wild-type and mutant forms. *Protein Expression Purif. 48*, 112–117.
27. Delaglio, F., Grzesiek, S., Vuister, G. W., Zhu, G., Pfeifer, J., and Bax, A. (1995) NMRPipe: A multidimensional spectral processing system based on Unix pipes. *J. Biomol. NMR 6*, 277–293.
28. Goddard, T. D., and Kneller, D. G. (2005) *Sparky*; University of California, San Francisco.
29. Barenholz, Y., Gibbes, D., Litman, B. J., Goll, J., Thompson, T. E., and Carlson, R. D. (1977) A simple method for the preparation of homogeneous phospholipid vesicles. *Biochemistry 16*, 2806–2810.
30. Huang, C.-h. (1969) Studies on Phosphatidylcholine Vesicles. Formation and Physical Characteristics. *Biochemistry 8*, 344–352.
31. Boettcher, J. M., Hartman, K. L., Ladror, D. T., Qi, Z., Woods, W. S., George, J. M., and Rienstra, C. M. (2007) ^{1}H, ^{13}C and ^{15}N resonance assignment of the cAMP-regulated phosphoprotein endosulfine-alpha in free and micelle-bound states. *Biomol. NMR Assignments 1*, 167–169.
32. Dyson, H. J., and Wright, P. E. (2004) Unfolded proteins and protein folding studied by NMR. *Chem. Rev. 104*, 3607–3622.
33. Wishart, D. S., and Sykes, B. D. (1994) The ^{13}C chemical-shift index: A simple method for the identification of protein secondary structure using ^{13}C chemical-shift data. *J. Biomol. NMR 4*, 171–180.
34. Cornilescu, G., Delaglio, F., and Bax, A. (1999) Protein backbone angle restraints from searching a database for chemical shift and sequence homology. *J. Biomol. NMR 13*, 289–302.
35. Rohl, C. A., and Baldwin, R. L. (1997) Comparison of NH exchange and circular dichroism as techniques for measuring the parameters of the helix-coil transition in peptides. *Biochemistry 36*, 8435–8442.
36. Huang, H. B., Chen, Y. C., Horiuchi, A., Tsai, L. H., Liu, H. T., Chyan, C. L., Hsieh, M. J., Liu, C. K., Lin, F. M., Greengard, P., Nairn, A. C., Shiao, M. S., and Lin, T. H. (2001) Letter to the Editor: Backbone ^{1}H, 15N, and ^{13}C resonance assignments of ARPP-19. *J. Biomol. NMR 19*, 383–384.
37. Sankaram, M. B., and Marsh, D. (1993) Protein-lipid interactions with peripheral membrane proteins, in *Protein-Lipid interactions* (Watts, A., Ed.) pp 127−158, Elsevier, Amsterdam.
38. Quesada, I., and Soria, B. (2004) Intracellular location of KATP channels and sulphonylurea receptors in the pancreatic beta-cell: new targets for oral antidiabetic agents. *Curr. Med. Chem. 11*, 2707–2716.
39. Schwanstecher, M., Schwanstecher, C., Dickel, C., Chudziak, F., Moshiri, A., and Panten, U. (1994) Location of the sulphonylurea receptor at the cytoplasmic face of the beta-cell membrane. *Br. J. Pharmacol. 113*, 903–911.
40. Wright, P. E., and Dyson, H. J. (1999) Intrinsically unstructured proteins: Re-assessing the protein structure-function paradigm. *J. Mol. Biol. 293*, 321–331.
41. Tompa, P., Szasz, C., and Buday, L. (2005) Structural disorder throws new light on moonlighting. *Trends Biochem. Sci. 30*, 484–489.

BI801450T